Al-Hunaiti A, Ghazzy A, Aqel H, Abu-Thiab T, Saeed R, Taha M, Hwaitat E, Zihlif M, Imraish A. New Chitosan-Based Trimetallic $Cu_{0.5}Zn_{0.5}Fe_2O_4$ Nanoparticles: Preparation, Characterization, and Anti-cancer activity. Pharmacy Practice. 2024 Oct-Dec;22(4):3016.
https://doi.org/10.18549/PharmPract.2024.4.3016

Original Research

New Chitosan-Based Trimetallic $Cu_{0.5}Zn_{0.5}Fe_2O_4$ Nanoparticles: Preparation, Characterization, and Anti-cancer Activity

Afnan Al-Hunaiti , Asma Ghazzy , Hazem Aqel ,Tuqa Abu-Thiab , Ramzi Saeed , Mutasem Taha , Eman Hwaitat , Malek Zihlif ,Amer Imraish

Received (first version): 25-Nov-2023 Accepted: 14-Feb-2024 Published online: 19-Nov-2024

Abstract

Objective: Develop a new nanomagnetic delivery system using trimetallic nanoparticles. **Results:** In this study, the structural morphology and the biological effects of magnetic $Cu_{0.5}Zn_{0.5}Fe_2O_4$ nanoparticles alone and with various coatings were investigated. The nanoparticles have shown a high potential biomedical application alone and as a targeted drug delivery system. The $Cu_{0.5}Zn_{0.5}Fe_2O_4$ nanoparticles were prepared by the phyto-mediated co-precipitation approach using *Boswellia carteri* resin aqueous extract. The synthesized nanoparticles underwent characterization through X-ray diffraction (XRD), Fourier transform infrared spectroscopy (FT-IR), and transmission electron microscopy (TEM). The XRD and TEM analysis revealed that the ultrafine nanoparticles were of size 20-85 nm. The coated NPs are chitosan-based, and the average nanoparticle size of polyethylene glycol (PEG) polymers was found to be 311-790 nm. The magnetic nanoparticles with the optimum particle size of 20 nm were then coated with chitosan and PEG polymer to form homogeneous suspensions. The hydrodynamic diameter and the polydispersity index (PDI) were analyzed by dynamic light scattering and were found to vary depending on the coating type. **Conclusion:** The MTT assay showed a relevant correlation between the size of the coated particles and the anti-cancer activity. Significantly, our data revealed a noteworthy correlation between coated particle size and anti-tumor reactivity, emphasizing the importance of optimizing particle size for enhanced cellular uptake. Notably, the plant extract used in nanoparticle synthesis exhibited a toxicity level of 134.57 µg/ml on fibroblasts, suggesting that the biological reactivity primarily originated from the metallic nanoparticles. The polymer coating effectively mitigated the toxicity of $Cu_{0.5}Zn_{0.5}Fe_2O_4$ nanoparticles on normal cells.

INTRODUCTION

Despite extensive global efforts, cancer remains a highly challenging disease and a leading cause of millions of deaths worldwide. While chemotherapy effectively targets cancer cells, its lack of precision often leads to harmful side effects in healthy tissues.[1] Patients undergoing treatments with such non-specific toxic compounds commonly experience severe side effects.[2] In this context, Magnetic nanoparticles (MNPs) hold the potential to transform existing clinical therapeutic and diagnostic methods. The application of MNPs in medical contexts represents a novel and interdisciplinary field with significant potential for diagnostic and therapeutic testing, both in vitro and in vivo.[3] Recently, MNPs have gained considerable attention as a valuable means in cancer therapy. These nanoparticles, including nickel, cobalt, and iron, possess ferromagnetic properties, which allow them to be directed by an external magnetic field.[4]

One of the most promising areas of research in cancer treatment focuses on delivering anti-cancer drugs through functionalized magnetic iron-based nanoparticles to specific target sites. The main challenge in chemotherapy lies in the lack of drug specificity, resulting in damage to both cancerous and healthy cells. To address this issue, controlled drug delivery using MNPs should maintain drug levels within the required concentration range for treatment, minimizing the risk of overdosing and reducing side effects.[5] Consequently, substances like chitosan, chitosan derivatives (e.g., chitosan phthalate), or PEG are increasingly recognized for their versatility in applications related to targeted drug delivery.[6,7] The utilization of nanoparticles has evolved beyond being mere drug delivery systems to also include mitigating the undesirable drug side effects.[8]

To date, various methods have been employed to synthesize ferrite-based nanoparticles. Among these methods, the co-precipitation method stands out as a valuable approach for efficiently producing a comparatively large quantity of nanoparticles using affordable and readily available chemical precursors.[9] Although the synthesis of trimetallic nanoparticles presents challenges compared to monometallic oxide or

Afnan AL-HUNAITI*. Department of Chemistry, The University of Jordan, Amman 11942, Jordan.
a.alhunaiti@ju.edu.jo
Asma GHAZZY. Faculty of Pharmacy, Al-ahliyya Amman University, Amman 19328, Jordan.
Hazem AQEL. Department of Micrbiology, Medicine School, Al-Balqa' Applied Univiersity, Salt 11222, Jordan.
Tuqa ABU-THIAB. Department of Biological Sciences, The University of Jordan, Amman 11942, Jordan.
Ramzi SAEED. Faculty of Pharmacy, The University of Jordan, Amman 11942, Jordan.
Mutasem TAHA. Faculty of Pharmacy, The University of Jordan, Amman 11942, Jordan.
Eman HWAITAT. Department of physics,The science school, The University of Jordan, Amman 11942, Jordan.
Malek ZIHLIF. Department of pharmacology, Medicin school The University of Jordan, Amman 11942, Jordan.
Amer IMRAISH. Department of Biological Sciences, The University of Jordan, Amman 11942, Jordan.
a.imraish@ju.edu.jo

bimetallic counterparts, recent research has reported successful co-precipitation synthesis of M-Zn ferrites.[11] Among the numerous techniques available for producing metallic nanoparticles, the co-precipitation method stands out for its appeal, as it permits operation at reduced temperatures and offers meticulous control over particle dimensions This method has been adopted in current research to synthesize copper–zinc ferrites ($Cu_xZn_{(x)}Fe_2O_4$) nanoparticles (CZFO).

Furthermore, the eco-friendly and cost-effective advantages of green synthesis, especially plant-based methods for iron-based NPs, have garnered significant attention.[10] Plant-mediated extracts contain a variety of compounds, including flavonoids, alkaloids, terpenoids, phenols, sugars, and proteins, which play a crucial role in reducing and stabilizing metal oxide nanoparticles.[12,13] here, we prepared CZFO nanoparticles using co-precipitation chemical method.[13] To mitigate the toxicity associated with ferrite nanoparticles, we incorporated biocompatible polymers, primarily chitosan and PEG with different particle sizes.[14-15] The presence of a polymer coating over CZFO NPs was tested for its anti-cancer activity against K562 leukemia, MDA.231, and MCF7 breast cancer cell lines.

MATERIALS AND METHODS

We utilized analytical-grade solvents from Aldrich in our experiments. These included medium molecular weight chitosan, polyethylene glycol with a molecular weight of 800, phenyl succinic anhydride (purchased from Sigma-Aldrich, USA), tripolyphosphate (TPA, sourced from Sigma-Aldrich, Germany), and phthalic anhydride (obtained from Fluka, Switzerland). Ultrapure water with a conductivity of 0.05 µs/cm was used for dynamic light scattering (DLS) size analysis, and it was obtained from Millipore, USA. For experimental purposes, we employed hydrochloric acid (37% concentration, from Fluka) and dialysis tubing with a molecular weight cutoff of 14 kDa (supplied by Sigma-Aldrich, USA). Tris base buffer was sourced from Bio Basic Inc., Canada. Additionally, $FeSO_4 \cdot 7H_2O$, $Zn(OAc)_2 \cdot 2H_2O$ and $CuSO_4.5H_2O$. Dichloro-methane (DCM, Fluka, Switzerland) and distilled water were used for the preparation of chitosan solutions.

Synthesis of copper-zinc ferrite $Cu_{0.5}Zn_{0.5}Fe_2O_4$ nanoparticles

Trimetallic ferrite nanoparticles were successfully prepared by utilizing an aqueous extract derived from *Boswellia Carteri resin*, following a previously established procedure.[13,16] Briefly, A mixture of 0.56 g of $FeSO_4.7H_2O$, 0.24 g of $Zn(OAC)_2.2H_2O$ and 0.24g $CuSO_4.5H_2O$ were dispersed in 20 mL of distilled water with continuous stirring for 2 h at room temperature to achieve a homogeneous solution. Subsequently, A 25 ml of aqueous plant extract was added dropwise to the reaction, and stirring was maintained for an additional hour. The pH was adjusted to achieve a pH level of 10 to 12. The resulting uniform solution was subjected to centrifugation, and the precipitate obtained was collected using magnetic filtration. These products were thoroughly washed with distilled water and ethanol. Finally, the samples were dried in a vacuum oven at 100°C for a duration of 6 hours.

Synthesis of chitosan-dicarboxylic acid derivative

The synthesis of Chitosan-phthalate nanoparticles (Chitosan-phthalate NPs) followed the previously reported method.[17] A 1.00 g of chitosan was dissolved in 50 ml of an aqueous solution containing 0.37% v/v HCl at room temperature. Simultaneously, 2.5 mmol of phthalic acid was dissolved in 5 ml of pyridine and added dropwise to the chitosan solution with vigorous stirring. To maintain the reaction pH at 7.0, a 1.0 M NaOH solution was gradually introduced into the reaction mixture. The reaction was allowed to proceed for 40 minutes. Afterward, the resulting chitosan derivative was precipitated by the slow addition of acetone while continuously stirring. The precipitate was then filtered and subjected to three washes with 100 ml portions of absolute ethanol, followed by a final wash with 100 ml of acetone. Subsequently, the product was dried for 48 hours in a hot air oven at 35°C. The resulting nanoparticles were stored in airtight containers.

Coating of trimetallic nanoparticle

The synthesis of chitosan-based nanoparticles (NPs), including both chitosan and chitosan-carboxylate NPs, was carried out using the previously established "syringe method".[18] In this process, chitosan or its derivative was dissolved by continuous stirring for 24 hours in an aqueous solution of HCl (4.8 mM) to create a 0.1% w/v solution. Subsequently, a freshly prepared aqueous solution of the crosslinker, namely TPP (0.4% w/v), was added drop by drop to the prepared solutions of chitosan or chitosan-carboxylate (5 ml each). For the synthesis of trimetallic nanoparticles (NPs), 10% by weight of NPs in relation to the polymer was added to the chitosan solution prior to sonication. Stirring continued until a visually apparent opalescent hazy dispersion was observed, indicating the formation of NPs. For PEG-modified trimetallic nanoparticles preparation, a 10 mM PEG solution was prepared by dissolving PEG in 50 ml of water. Subsequently, 20 mg of $Cu_{0.5}Zn_{0.5}Fe_2O_4$ nanoparticles were introduced into the PEG solution and subjected to 24 hours of ultrasonication. Afterward, the solutions were centrifuged for 20 minutes, and any excess chitosan or PEG solution was carefully removed. The resulting nanoparticles were utilized for size and zeta potential analysis, specifically through dynamic light scattering (DLS), without additional treatment.

Characterization

The examination of CZFO nanoparticles included an evaluation of their morphology and crystalline structure Field emission scanning electron microscopy (SEM, FESEM JEOL JSM-6380) was employed for morphological analysis, while X-ray powder diffraction (XRD) analysis, using an X'pert diffractometer with CuK α radiation, was conducted to evaluate the crystalline structure. Additionally, the hydrodynamic particle size and size distribution of these nanoparticles were determined through dynamic light scattering (DLS) measurements, utilizing a Zetasizer Nano-ZSP instrument from Malvern Instruments in Worcestershire, UK. These measurements were performed at a consistent room temperature of 25±2°C. For the analysis, the nanoparticle suspensions were diluted with distilled water at a 1:20 (v/v) ratio and loaded into a cuvette. Moreover, the

Zeta potential of the suspended nanoparticles was determined using the electrophoretic light scattering (ELS) technique. Size measurements were taken accordingly. The polydispersity index (PDI), which serves as an indicator of size distribution, was also determined. The zeta potential measurements for CS, PEG, and phthalyl CS NPs were performed in triplicate and are presented as the mean ± standard deviation (SD).

Cell culture and maintenance

To assess the potential anticancer properties of our biosynthesized nanoparticles (NPs), we employed the Polydispersity Index (PDI) as an indicator of NP size distribution. These NPs were tested on various types of cells, including K562 human leukemia (ATCC® CCL-243™, USA), MDA-MB-231 human breast cancer (ATCC® CRM-HTB-26™, USA), MCF7 human breast cancer cell line (ATCC® HTB-22™, USA), and human skin fibroblast (ATCC® PCS-201-012™). The cells were cultured and maintained in a controlled environment at 37 °C with 5% CO2. Specifically, K562 and MCF7 cells were cultured in RPMI-1640 (Euroclone), For the cell lines, Dulbecco's Modified Eagle Medium (DMEM; Gibco) was utilized, except for the remaining cell lines where the same culture medium was employed. Both culture media were enhanced with 10% fetal bovine serum (Gibco), 1% penicillin-streptomycin (Euroclone), and 1% L-Glutamine (Euroclone).

Cytotoxicity and anticancer potential investigation

Cells were seeded in a 96-well plate with a seeding density 7×103 for MDA-MB-231 and MCF7, 10×103 for fibroblast, and 15×103 for K562. Cells were incubated overnight to attach and then treated with a serial dilution of each NP, where 100 µg/ml was the highest concentration and 1.6 µg/ml was the lowest. A stock solution of 10 mg/ml of each NP was prepared; they were dissolved in 99.5% dimethyl sulfoxide and 0.5% 5 M nitric acid to enhance their solubility and then further subjected to ultrasonication for 30 mins at room temperature. Taking into consideration DMSO toxicity on cells, its percentage did not exceed 1% for all treatments, which is safe and approved for cells. Control cells were running through each experiment. After 72 hours of treatment, a MTT cell viability assay was performed using Cell Titer 96 ® Non-Radioactive Cell Proliferation Assay (Promega, USA), and optical densities (ODs) were measured at 570 nm. GraphPad Prism software was used to determine the IC_{50} value of each tested nanoparticle.

Statistical analysis

The experimental findings were presented as the mean values along with their corresponding standard deviations (SD). Microsoft Excel software (Microsoft Corp., Redmont, WA, USA) was used to calculate the means, standard deviations for size, zeta potential, loading amount, cumulative amount released, and to generate graphical representations. The determination of IC50 values for each set of tested nanoparticles was accomplished by employing the logarithmic trend line of cytotoxicity graphs (log [concentration vs inhibition]) with the assistance of GraphPad Prism 8 software from GraphPad Software, Inc.

RESULTS AND DISCUSSION

Trimetallic

The X-ray diffraction (XRD) patterns of all CZFO samples are presented in Figure 1. Within these XRD patterns, distinct peaks corresponding to crystallographic planes (220), (311), (400), and (511) were detected and exhibited excellent conformity. Examination of the CZFO nanoparticles disclosed an average crystallite size of around 85 nm. To ascertain the lattice constant and crystallite size, Scherrer formula was employed, centered on the most prominent peak observed at (311).[18]The X-ray diffraction patterns further confirmed that the CZFO nanoparticles exhibit a single-phase spinel arrangement without any ambiguity. The experimentally obtained d-spacing values and relative intensities closely matched those documented in the literature. Specifically, the XRD spectra displayed d-spacing values of 2.98, 2.54, and 2.11, which were consistent with the standard XRD pattern. Additionally, the lattice parameters fell within the expected range for $Cu_xZn_{(1-x)}Fe_2O_4$ nanoparticles.[19-21]

The XRD patterns along with the Rietveld refinement for the $Cu_{0.5}Zn_{0.5}Fe_2O_4$ sample are illustrated in Figure 1. Rietveld analysis of the $Cu_{0.5}Zn_{0.5}Fe_2O_4$ sample's pattern confirmed the presence of a predominant cubic (fcc) spinel phase, consistent with the standard pattern of $Cu_{0.5}Zn_{0.5}Fe_2O_4$ phase (JCPDS: 00-051-0386) and CuO (JCPDS: 00-041-0254). The reflections associated with the spinel phase are labeled with their respective Miller indices (hkl). The relatively low values of the reliability factors (RB and RF) and the good fit (χ2) indicates a reliable fit as demonstrated by the (almost) horizontal difference curve (blue line in Figure 1)).

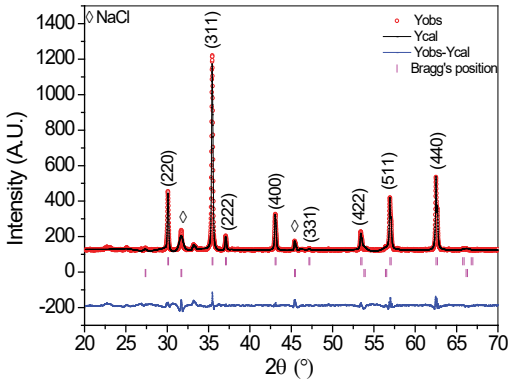

Figure 1. XRD patterns with Rietveld refinement for $Cu_{0.5}Zn_{0.5}Fe_2O_4$ NPs

The refined lattice parameters (a) and the cell volume V of the spinel phase were obtained by fitting the XRD patterns which are listed in Table 1. The lattice constant is a = 8.40 Å which is consistent with the reported values of 8.34-8.41 Å.[18]

The measured cell volume (V) recorded a value of 592.2 Å³. The theoretical X-ray density for each specimen was calculated based on the number of molecules (Z = 8) within the unit cell,

$$\rho_x = \frac{Z(M_w)}{N_A V} \quad (1)$$

Here N_A is Avogadro's number. The theoretical X-ray density was 5.37 g/cm^3.

The crystallite size (D) of each sample was calculated using the Stokes–Wilson equation.[19-20]

$$D = \frac{\lambda}{\beta_c \cos\theta} \quad (2)$$

where λ is the X-ray wavelength (0.15406 nm), θ is the Bragg's angle of diffraction in degrees, and βc is the integral breadth of the diffraction peak corrected for the instrumental broadening. The diffraction peak used for the determination of the crystallite size was fitted with Lorentzian line-shape, and the integral breadth was determined by the relation.

$$\beta = \frac{A}{I_O} \quad (3)$$

the crystallite size of the CZFO nanoparticles using peak area (A) and maximum intensity (I_0) data. Specifically, we focused on the most intense peak (311) at 2θ = 35.6° to determine the crystallite size perpendicular to the corresponding crystallographic plane. Additionally, we assessed the crystallite size of the spinel phase along different crystallographic directions, including the (220) reflection at 2θ = 30.0° and the (400) reflection at 43.04°. The results of these crystallite size measurements for the spinel phase are presented in Table 2. It is evident that the crystallite size perpendicular to the (220) planes is larger than those along other directions, suggesting a platelet-like shape for the crystallites.

Table 1. Lattice Parameters, Cell Volume, X-ray Density, Reliability Factors and Goodness of Fit (RB, RF, and χ2 for the Cu0.5Zn0.5Fe2O4 NPs)

Phase	a (Å)	V (Å^3)	(g/cm^3)	R_B	R_F	χ^2
$Cu_{0.5}Zn_{0.5}Fe_2O_4$	8.40	592.2	5.37	0.679	0.644	0.270

Table 2. Crystallite size of spinel phase along different crystallographic directions

sample	Crystallite size(D) nm		
	(220)	(311)	(400)
$Cu_{0.5}Zn_{0.5}Fe_2O_4$	285	231	88

We also examined the morphology of the synthesized CZFO nanoparticles using SEM images, as depicted in Figure 2. The SEM images illustrate the variations in morphology among different samples, including CZFO without additives, CZFO with PEG, CZFO with CS, and CZFO with phthalyl CS. Figure 2 shows the diffraction pattern of the PEG-chitosan- $Cu_{0.5}Zn_{0.5}Fe_2O_4$ sample prepared at room temperature. This pattern is consistent with the standard patterns from the JCPDS database: PEG phase at 23.48° and 26.1°, chitosan phase (JCPDS: 00-039-1894) at 20.4°, 24°, and 26.1°, $Cu_{0.5}Zn_{0.5}Fe_2O_4$ phase at 30.0°, 35.4°, 43.1°, 53.5°, 57.0°, and 62.4°, as well as ZnO and CuO phases.

Comparing the XRD pattern of $Cu_{0.5}Zn_{0.5}Fe_2O_4$ nanoparticles (Figure 2a) with the structural patterns of core nano $Cu_{0.5}Zn_{0.5}Fe_2O_4$ particles surface-capped with phthalyl CS and PEG chitosan (Figures 2b and 2c, respectively), it is evident that the surface-capping agents weaken the intensity of core peaks. This effect is attributed to the capping agents masking the metallic nanoparticles core.

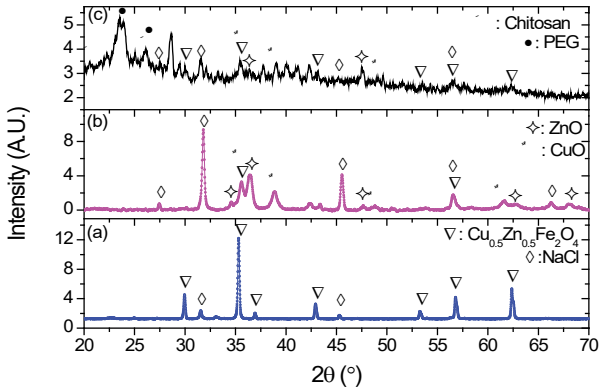

Figure 2. XRD patterns of (a) CZFO sample, (b) pthalyl CS-CZFO sample, (c) PEG -CZFO sample

NPs size analysis, surface charge measurement, and stability studies under variable pH, $CaCl_2$ conditions

We examined dispersions of coated nanoparticles (NPs) using dynamic light scattering (DLS) under various conditions. This evaluation was performed directly at the initial pH and after exposure to different pH levels (1.2, 6.8, 7.4, and 12.0), as well as various $CaCl_2$ concentrations (0.1, 0.2, 0.3, 0.4, and 0.5 M) to assess the stability of the particles. pH adjustments were made using either aqueous NaOH (0.1 M) or HCl (1.0 M), and pH levels were monitored with a pH-meter (Hanna, USA). Prior to DLS analysis, each sample was stirred for 3 minutes at room temperature to ensure a uniform dispersion.

We determined the particle size, polydispersity index (PDI), and zeta potential by assessing the electrophoretic mobility of NP dispersions and applying the Stokes-Einstein and Henry equations. The calculations considered specific parameters, including the media viscosity (0.8872 cP), dielectric constant (78.5), and temperature (25 °C). These calculations were executed using ZetaSizer software version 7.11, with measurements conducted in triplicate at 25 °C, and the resulting average values for size and zeta potential were recorded in Table 3, we prepared coated NPs of various sizes and tested their stability under different conditions. The Chitosan-phthalate-CZFO1 and CZFO2 displays a robust pH stability range with values recorded at 360, 366, and 457 nm, suggesting that this formulation maintains a stable size across different conditions, making it a potentially good candidate for environments with fluctuating pH, such as the gastrointestinal tract. Comparing the same type of coating but with two different size ranges (Chitosan -phthalyl and PEG), we observed that larger sizes in both cases exhibited lower stability in terms of pH and $CaCl_2$ concentration. Aggregation occurred at lower pH levels (around pH 6.4) and $CaCl_2$ concentrations of 0.2 M

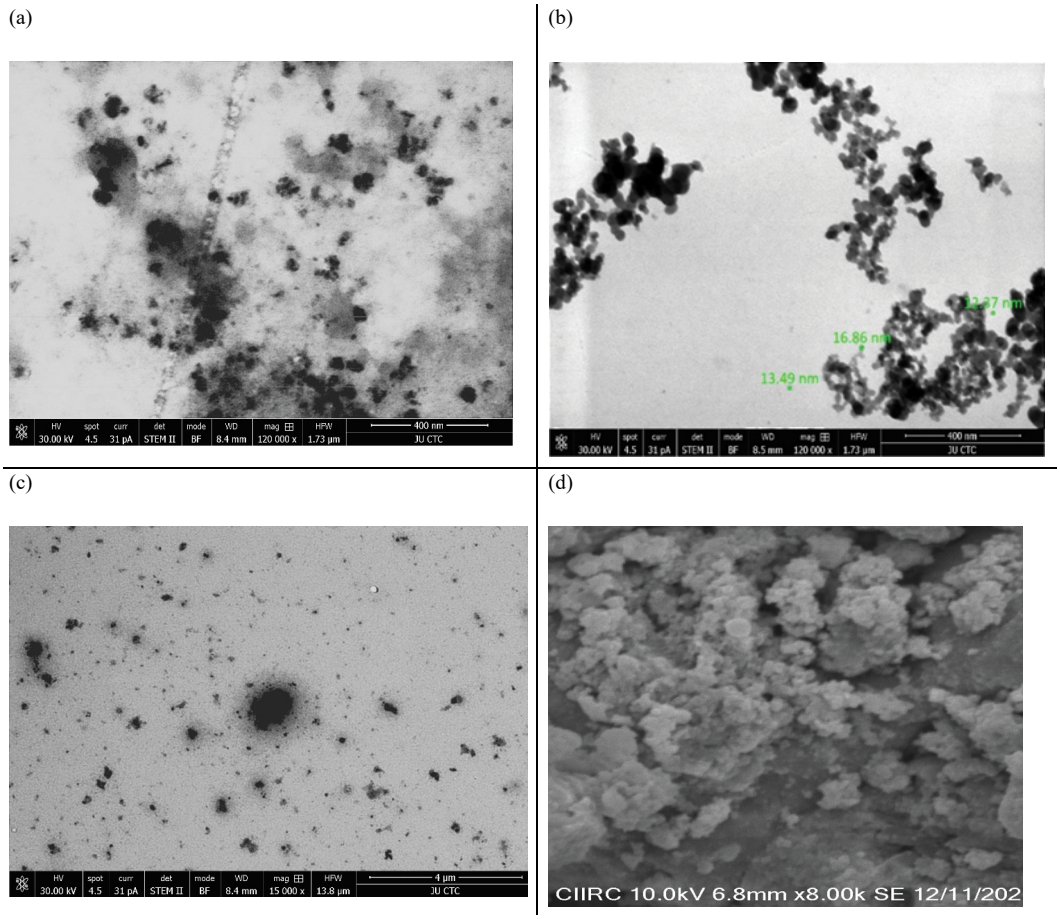

Figure 3. SEM of CZFO nanoparticles, (a) free CZFO Nps without coating (b) CZFO NP with PEG (c) pthalyl CS-CZFO with (e) PEG-CZFO Np with Chitosan

or higher. This behaviour can be attributed to the chelation interactions between Ca^{2+} ions and phosphate ions present within the coating polymer linkers.

Interestingly, when comparing different types of coated CZFO NPs, we found that PEG and the modified Chitosan (phthalyl CS) coatings offered better stability compared to unmodified chitosan (CS) and the free nanoparticles. Moreover, in terms of zeta potential, it was significantly influenced by the type of coating polymer used in the NPs fabrication process. The free NPs exhibited the highest value, which decreased substantially when coated with PEG and phthalate CS, with values of 4.2 and 2.2, respectively. Notably, the $CaCl_2$ test was not applied to PEG-coated NPs since no phosphoamide linkers were used. our findings indicate that the size and type of coating play critical roles in the stability of nanoparticles under varying environmental conditions. Notably, the Chitosan-phthalate-CZFO formulations exhibited promising stability across different pH levels, making them suitable candidates for applications in complex biological systems, such as drug delivery within the gastrointestinal tract. The stability trends observed in relation

Table 3. The variation of average diameter(Dav),polydispersity index (PDI), pH stability and $CaCl_2$ with different Np coating

NPs names	Sizes [a]	PDI [a,b]	pH stability [nm] 1.2 6.8 7.4 12	$CaCl_2$ stability [nm] 0.1 0.2 0.3 0.5	Z-potential
Chitosan- CZFO	317.6±10.67	0.188±0.085	390 -- -- --	-- -- -- --	-12.1
Chitosan-phthalate- CZFO2	696.9±75.6	0.270±0.16	--- -- -- --	--- -- -- --	-2.2
Chitosan-phthalate - CZFO1	311.3±5.7	0.134±0.03	360 366 457 --	460 -- -- --	-28.5
PEG- CZFO2	411.3±28.8	0.120±0.044	580 599 673 --	ND	-4.8
PEG- CZFO1	317.3±10.04	0.136±0.032	421 454 665 --	ND	-25.2
CZFO free	78±10.04	0.13±0.03	0.027 0.05 0.1 --	0.028 0.83 -- --	-23

[a] Each point represents at least duplicate measurements ± standard deviation.
[b] Polydispersity index.
(ND: not studied, --: aggregate).

to particle size and ionic concentration emphasize the necessity for careful consideration of these factors in the design and application of nanoparticle-based systems. After characterizing the synthesized NPs in terms of particle size, zeta potential, and stability in $CaCl_2$ and pH, we investigated their effects using different cell lines in MTT assays.

MTT assay

To evaluate the biocompatibility and anti-cancer potential of the newly synthesized nanoparticles, we conducted experiments using different concentrations of each nanoparticle on various cell lines, including K562 leukemia, MDA.231, MCF7 breast cancer cell lines, and normal fibroblast skin cells. Table 4 presents the half-maximal inhibitory concentration (IC_{50}) values for each tested nanoparticle on the different cell lines. As depicted in the table, CZFO-free nanoparticles exhibited strong cytotoxic effects on the MCF7 breast cancer cell line, with an IC_{50} value of 4.4 µg/ml, and showed cytotoxicity against K562 leukemia cells, with an IC_{50} value of 19.7 µg/ml. Notably, the impact of CZFO-free nanoparticles varied across different cell lines, and its cytotoxic effect was approximately four times weaker on leukemia cells compared to its effect on MCF7 cells. Moreover, CZFO-free nanoparticles demonstrated no toxicity towards MDA.231 breast cancer cells or normal fibroblast cells, as their IC_{50} values exceeded 100 µg/ml.

The potent and selective effect of the prepared nanoparticles, which is more pronounced in MCF7 cells and less evident in leukemia cells while remaining safe for normal cells, is the strength point of the prepared system. This suggests their potential as a powerful anti-cancer therapy that selectively targets specific cancer types without harming normal tissues, addressing a significant challenge associated with conventional chemotherapy approaches.

Furthermore, both Chitosan-phthalate- CZFO and PEG-CZFO nanoparticles exhibited significant anti-cancer efficacy against the K562 cell line at nanomolar concentrations, with IC_{50} values of approximately 420 ng/ml and 500 ng/ml, respectively. While PEG-CZFO maintained its strong anti-cancer effect against the MDA.231 and MCF7 cancer cell lines, it was still approximately three times weaker in these cases compared to its effect on K562 cells, suggesting potential variability in its cancer targeting. On the other hand, Chitosan-phthalate-CZFO1 exhibited a similar effect on both MDA.231 and MCF7 breast cancer cell lines, with IC_{50} values approximately 14 times higher than the IC_{50} value observed on K562 cells. These findings imply that Chitosan-phthalate-CZFO1 demonstrates selective activity towards K562, possibly targeting a specific receptor highly expressed in K562 cells compared to other cancer types.

Interestingly, both Chitosan-phthalate- CZFO1 and PEG-CZFO nanoparticles showed moderate toxicity towards normal fibroblasts, with IC_{50} values of 23.9 µg/ml and 16.6 µg/ml, respectively. These IC_{50} values were significantly higher, approximately 57 and 33 times higher, respectively than the IC_{50} values observed on K562 cell lines. Although their reduced biocompatibility limits their broad biological applications, considering their selectivity towards K562 cells, they can be employed at extremely low concentrations to eliminate this specific type of cancer without harming normal tissue. In contrast, PEG-CZFO and CS-CZFO nanoparticles exhibited safety on all tested cell lines, with IC_{50} values exceeding 100 µg/ml. Their biocompatibility could be utilized for other biological applications, such as anti-inflammatory or antioxidant activities. As for Chitosan-phthalate- CZFO, it displayed a promising selective anti-cancer effect primarily against K562 leukemia carcinoma, with an IC_{50} value approximately 13.4-fold lower than that observed on fibroblasts, ensuring safety towards normal tissues and strong selectivity towards leukemia carcinoma when used at very low concentrations.

When we compare the biological reactivity with the type of coating and the NPs size, we find that CS doesn't provide a proper coat for such type of metallic oxides (trimetallic oxide) as it shows the lowest biological activity (CS-CZFO). Furthermore, a relevant correlation between nanoparticle size and their IC_{50} level. Both PEG and phthalyl have low IC_{50} on various cancer lines when the size ~300 (particles 2 and 3);meanwhile, when the NP size increases,a lower reactivity (PEG-$CZFO_2$ and chitosan phthalate- $CZFO_2$) is shown. This observation matches with previous reports where specific particle size is needed to improve the NPs cellular uptake.[21]-24 Noteworthy, the plant extract used in the preparation of the trimetallic nanoparticles showed 134.57 µg/ml on the fibroblast, which leads us to believe that biological reactivity mainly came from the metallic nanoparticles and the polymer coating allowed for the reduction of the toxicity of CZFO Nps on the normal cell.

Table 4. IC_{50} of NPs on K562 leukemia, MDA.231, MCF7 breast cancer cell lines and fibroblast normal skin cells

NP type\ Cell line	Size (nm)	K562 (µg/ml±SEM)	MDA.231 (µg/ml±SEM)	Fibroblast (µg/ml±SEM)	MCF7 (µg/ml±SEM)
CZFO-free	78	>100	>100	>100	>100
Chitosan- phthalate -CZFO1	311	0.42±0.02	5.3±0.05	23.9±0.04	6.4±0.04
PEG-CZFO1	317	0.5±0.01	1.7±0.02	16.6±0.12	1.4±0.07
PEG-CZFO2	411	>100	>100	>100	>100
CS-CZFO	317	>100	>100	>100	>100
Chitosan- phthalate -CZFO2	696	13.4±0.22	76±0.11	55.3±0.34	>100
Boswellai carteri resin aqueous extract	---	53.4±0.04	93.74±0.02	134.57±0.01	245.7±0.03

CONCLUSIONS

In conclusion, the nanoparticles exhibit significant potential for biomedical applications both independently and as part of targeted drug delivery systems. We successfully prepared $Cu_{0.5}Zn_{0.5}Fe_2O_4$ nanoparticles using a phyto-mediated co-precipitation approach with an aqueous extract of Boswellia Carteri resin. The characterization of these nanoparticles involved XRD, FT-IR, and TEM analyses. The XRD and TEM analyses revealed that the ultrafine nanoparticles ranged in size from 2 to 22 nm. These nanoparticles were coated with chitosan-based and PEG polymers, resulting in average nanoparticle sizes of 311-790 nm. The magnetic nanoparticles, with an optimum particle size of 78 nm, were further coated with chitosan and PEG polymers to form homogeneous suspensions. Dynamic light scattering analysis at a physiological temperature of 37°C indicated hydrodynamic diameters of 317 nm to 790 nm for chitosan-based coated nanoparticles and 311 nm to 420 nm for PEG-coated ones. The coated nanoparticles demonstrated excellent stability under various conditions, including pH variations and varying $CaCl_2$ concentrations. Both chitosan phthalate and PEG-coated particles exhibited proper physicochemical stability. In terms of anti-cancer studies (MTT studies), both phthalyl and PEG coatings exhibited potent anticancer effects against the K562 cell line at nano concentrations, with IC_{50} values of approximately 420 and 500 ng/ml, respectively. Furthermore, the coated nanoparticles, phthalyl, and PEG, showed moderate toxicity toward normal fibroblasts, with IC_{50} values of 23.9 and 16.6 µg/ml, respectively.

Furthermore, it is important to highlight that the plant extract used in the preparation of the trimetallic nanoparticles exhibited a toxicity level of 134.57 µg/ml on fibroblasts, suggesting that the biological reactivity primarily stemmed from the metallic nanoparticles. The polymer coating effectively mitigated the toxicity of CZFO NPs on normal cells. Notably, the data obtained revealed a significant correlation between the coated particle size and its anti-tumor reactivity, indicating that an optimal particle size enhances cellular uptake; above the optimal size, the reactivity of the Np reduced or even demolished completely. To gain a comprehensive understanding of biological reactivity, further investigations into biodegradability and elimination are currently underway before considering the clinical application of this system.

AUTHOR CONTRIBUTIONS

A. Al-Hunaiti: Writing– review and editing, Writing– original draft, Project administration, A. M. Ghazzy: Investigation, Aqel H: Conceptualization and Formal analysis. T. Abu-Thiab: Investigation, R. Saeed: Validation, M. Taha; Conceptualization, E. Hwaitat: Formal analysis, M.Zihlif: Project administration, ,A. Imraish: Writing– review and editing, Writing– original draft.

CONFLICTS OF INTEREST

There are no conflicts to declare.

ACKNOWLEDGEMENTS

This work was supported by a grant from the Deanship of Scientific Research at the University of Jordan.

References

1. Pon-On W, Tithito T, Maneeprakorn W, Phenrat T, Tang IM. Investigation of magnetic silica with thermoresponsive chitosan coating for drug controlled release and magnetic hyperthermia application. Materials Science and Engineering: C. 2019;97:23-30. https://doi.org/10.1016/j.msec.2018.11.076
2. Gaware SA, Rokade KA, Kale SN. Silica-chitosan nanocomposite mediated pH-sensitive drug delivery. Journal of Drug Delivery Science and Technology. 2019;49:345-51.
3. Hassan HA, Diebold SS, Smyth LA, Walters AA, Lombardi G, Al-Jamal KT. Application of carbon nanotubes in cancer vaccines: achievements, challenges and chances. Journal of controlled release. 2019;297:79-90. https://doi.org/10.1016/j.jconrel.2019.01.017
4. Sharmeen S, Rahman AM, Lubna MM, Salem KS, Islam R, Khan MA. Polyethylene glycol functionalized carbon nanotubes/gelatin-chitosan nanocomposite: An approach for significant drug release. Bioactive materials. 2018;3(3):236-44. https://doi.org/10.1016/j.bioactmat.2018.03.001
5. Bediako EG, Nyankson E, Dodoo-Arhin D, Agyei-Tuffour B, Łukowiec D, Tomiczek B, et al. Modified halloysite nanoclay as a vehicle for sustained drug delivery. Heliyon. 2018;4(7):e00689. https://doi.org/10.1016/j.heliyon.2018.e00689
6. Argüelles-Monal WM, Lizardi-Mendoza J, Fernández-Quiroz D, Recillas-Mota MT, Montiel-Herrera M. Chitosan derivatives: Introducing new functionalities with a controlled molecular architecture for innovative materials. Polymers. 2018;10(3):342. https://doi.org/10.3390/polym10030342
7. Amiri M, Salavati-Niasari M, Akbari A. Magnetic nanocarriers: evolution of spinel ferrites for medical applications. Advances in colloid and interface science. 2019;265:29-44. https://doi.org/10.1016/j.cis.2019.01.003
8. Rainone P, Riva B, Belloli S, Sudati F, Ripamonti M, Verderio P, et al. Development of 99mTc-radiolabeled nanosilica for targeted detection of HER2-positive breast cancer. International journal of nanomedicine. 2017;12:3447. https://doi.org/10.2147/ijn.s129720
9. Ahamed M, Akhtar MJ, Alhadlaq HA, Khan MM, Alrokayan SA. Comparative cytotoxic response of nickel ferrite nanoparticles

in human liver HepG2 and breast MFC-7 cancer cells. Chemosphere. 2015;135:278-88. https://doi.org/10.1016/j.chemosphere.2015.03.079
10. Khanna L, Gupta G, Tripathi SK. Effect of size and silica coating on structural, magnetic as well as cytotoxicity properties of copper ferrite nanoparticles. Materials Science and Engineering: C. 2019;97:552-66. https://doi.org/10.1016/j.msec.2018.12.051
11. Tzankov B, Tzankova V, Aluani D, Yordanov Y, Spassova I, Kovacheva D, et al. Development of MCM-41 mesoporous silica nanoparticles as a platform for pramipexole delivery. Journal of Drug Delivery Science and Technology. 2019;51:26-35.
12. Imraish A, Abu Thiab T, Al-Awaida W, Al-Ameer H.J, Bustanji Y, Hammad H, Alsharif M, Al-Hunaiti A.
1. In vitro anti-inflammatory and antioxidant activities of ZnFe2O4 and CrFe2O4 nanoparticles synthesized using Boswellia carteri resin, J. Food Biochem.2021, p. 6.
13. Wen X, Yang F, Ke QF, Xie XT, Guo YP. Hollow mesoporous ZSM-5 zeolite/chitosan ellipsoids loaded with doxorubicin as pH-responsive drug delivery systems against osteosarcoma. Journal of Materials Chemistry B. 2017;5(38):7866-75. https://doi.org/10.1039/c7tb01830d
14. Wang G, Zhao D, Ma Y, Zhang Z, Che H, Mu J, et al. Synthesis and characterization of polymer-coated manganese ferrite nanoparticles as controlled drug delivery. Applied Surface Science. 2018;428:258-63.
15. Chen C, Yao W, Sun W, Guo T, Lv H, Wang X, et al. A self-targeting and controllable drug delivery system constituting mesoporous silica nanoparticles fabricated with a multi-stimuli responsive chitosan-based thin film layer. International journal of biological macromolecules. 2019;122:1090-9. https://doi.org/10.1016/j.ijbiomac.2018.09.058
16. Imraish A, Al-Hunaiti A, Abu-Thiab T, Ibrahim Al-Qader A, Hwaitat E, Omar A, Phyto-Facilitated Bimetallic ZnFe2O4 Nanoparticles via Boswellia carteri: Synthesis, Characterization, and Anti-Cancer Activity, Anti-Cancer Agents in Medicinal Chemistry; 2021Volume 21, Issue 13, DOI: 10.2174/1871520621666201218114040
17. Saeed RM, Dmour I, Taha MO. Stable chitosan-based nanoparticles using polyphosphoric acid or hexametaphosphate for tandem ionotropic/covalent crosslinking and subsequent investigation as novel vehicles for drug delivery. Frontiers in bioengineering and biotechnology. 2020;8:4. https://doi.org/10.3389/fbioe.2020.00004
18. Imraish, A., Zihlif, M., Thiab, T. A., Al-Awaida, W., Al-Ameer, H. J., & Al-Hunaiti, A. (2024). Anti-Inflammatory and Antioxidant Effects of Rosmarinic Acid Trimetallic (Cu0.5Zn0.5Fe2O4) Nanoparticles. Chemistry & Biodiversity, 21(5), e202301739. https://doi.org/10.1002/cbdv.202301739
19. Bhavsar D, Gajjar J, Sawant K. Formulation and development of smart pH responsive mesoporous silica nanoparticles for breast cancer targeted delivery of anastrozole: In vitro and in vivo characterizations. Microporous and Mesoporous Materials. 2019;279:107-16.
20. Szegedi Á, Shestakova P, Trendafilova I, Mihayi J, Tsacheva I, Mitova V, et al. Modified mesoporous silica nanoparticles coated by polymer complex as novel curcumin delivery carriers. Journal of Drug Delivery Science and Technology. 2019;49:700-12.
21. Phadatare MR, Khot VM, Salunkhe AB, Thorat ND, Pawar SH. Studies on polyethylene glycol coating on NiFe2O4 nanoparticles for biomedical applications. Journal of Magnetism and Magnetic Materials. 2012;324(5):770-2. https://doi.org/10.3390/nano11020440
22. Jermy BR, Acharya S, Ravinayagam V, Alghamdi HS, Akhtar S, Basuwaidan RS. Hierarchical mesosilicalite nanoformulation integrated with cisplatin exhibits target-specific efficient anticancer activity. Applied Nanoscience. 2018;8(5):1205-20.
23. Liu WT, Yang Y, Shen PH, Gao XJ, He SQ, Liu H, et al. Facile and simple preparation of pH-sensitive chitosan-mesoporous silica nanoparticles for future breast cancer treatment. Express Polymer Letters. 2015;9(12).
24. Tang L, Yang X, Yin Q, Cai K, Wang H, Chaudhury I, et al. Investigating the optimal size of anticancer nanomedicine. Proceedings of the National Academy of Sciences. 2014;111(43):15344-9. https://doi.org/10.1073/pnas.1411499111

www.pharmacypractice.org (eISSN: 1886-3655 ISSN: 1885-642X)